PHOTONIC SENSORS / Vol. 9, No. 2, 2019: 189–196

A Coil Constant Calibration Method Based on the Phase-Frequency Response of Alkali Atomic Magnetometer

Han YAO, Danyue MA, Junpeng ZHAO, Jixi LU, and Ming DING*

School of Instrumentation Science and Opto-electronics Engineering, Beihang University, Beijing 100191, China

*Corresponding author: Ming DING E-mail: mingding@buaa.edu.cn

Abstract: We propose an *in-situ* method to calibrate the coil constants of the optical atomic magnetometer. This method is based on measuring the Larmor precession of spin polarized alkali metal atoms and has been demonstrated on a K-Rb hybrid atomic magnetometer. Oscillation fields of different frequencies are swept on the transverse coil. By extracting the resonance frequency through phase-frequency analysis of electron spin projection, the coil constants are calibrated to be 323.1 ± 0.28 nT/mA, 108 ± 0.04 nT/Ma, and 185.8 ± 1.03 nT/mA along the X, Y, and Z directions, respectively.

Keywords: Optical atomic magnetometer; coil constant calibration; phase-frequency analysis; Larmor precession

Citation: Han YAO, Danyue MA, Junpeng ZHAO, Jixi LU, and Ming DING, "A Coil Constant Calibration Method Based on the Phase-Frequency Response of Alkali Atomic Magnetometer," *Photonic Sensors*, 2019, 9(2): 189–196.

1. Introduction

Atomic magnetometer, with the rapid development of recent decades [1–3], has been reported as the most sensitive known magnetic measurement instrument. It has found many applications such as geomagnetism [4], medical imaging [5, 6], and fundamental physics [7, 8]. At least, one set of triaxial magnetic coil system is required in the magnetometer to supply direct current (DC) or alternating current (AC) field. The accuracy of its coil constant always has significant effects on the overall performance of the atomic magnetometers.

A uniform and pure magnetic environment is essential while passive magnetic shielding barrels alone can hardly manage it without the accurate offset fields generated by the coil system. On one hand, the residual magnetic field cannot be adequately compensated without accurate coil constants. Taking spin-exchange relaxation free (SERF) regime as an instance, one elementary premise of its ultra-high sensitivity is extremely weak surrounding field at the level of several nT. On the other hand, accurate coil constants are also important when large ambient field of several pT is generated by the coils [9]. Considering the relatively large current applied, significant discrepancy may emerge when the coil constants deviate from the original values. Thus, a convenient *in-situ* coil constants calibration operation is necessary from this point. Apart from these, accurate coil constants decide the direct readout of the atomic magnetometers working in the close-loop mode. In these kinds of magnetometers, magnetic fields have to be maintained to particular values to satisfy the underlying physics, such as the steady-state operating point and the resonance point, or to

Received: 30 August 2018 / Revised: 19 November 2018

DOI: 10.1007/s13320-019-0530-4
Article type: Regular

increase the dynamic range and bandwidth of the magnetometer. Through feedback control, the magnitudes of the external magnetic fields are actually obtained in real time from the compensation value of coils [9–12].

In addition to DC magnetic fields, the coil system serves to produce accurate AC magnetic fields of various functions. One most elementary part is to generate the known reference signal for the sensitivity estimation of the magnetometer. The importance of coil constant accuracy for this purpose is much in evidence. Moreover, modulation fields are often applied to measure magnetic fields along two or three axes. In the case of longitudinal parametric modulation, the magnitude of normalized oscillation field determines not only the response strength, but also the loss of bandwidth [13]. Thus, accurate magnetic fields from the longitudinal coil directly affect the optimization of such kind of magnetometer. As to transverse AC modulation, its field magnitude is exactly the scale factor between the demodulated signal and the field to be measured. Under this circumstance, calibrating coil constants ties in nicely with calibrating the magnetometer response [14].

Above all, a precise method should be designed to calibrate the magnetic coil constants and obtain the accurate value of the applied magnetic field.

Using a fluxgate to measure the magnetic field in the center of the coil system is a traditional method for calibrating the coil constant [15]. However, its accuracy is limited by the placement error and the precision of fluxgate. An *in-situ* method developed by Zhang *et al.* can measure the magnetic coil constants based on the Larmor precession frequency of the hyperpolarized ^{3}He [16]. Chen *et al.* proposed another calibration method by measuring the initial amplitude of free induction decay (FID) of ^{129}Xe and calculating the $\pi/2$ pulse duration [17]. Both of these methods require to operate with noble gas atoms due to their long polarization lifetime and are suitable for spin-precession gyroscopes and co-magnetometers, while they are not suitable for atomic magnetometers using alkali metal atoms as sensing unit.

This paper presents an *in-situ* calibration method based on the Larmor precession of the polarized alkali metal atoms. It is demonstrated in a K-Rb hybrid atomic magnetometer. The electron spins are pumped in the vapor cell and functioned as the sensing unit of the atomic magnetometer. Then, the phase-frequency response of the magnetic resonance is analyzed, and the Larmor precession frequency of the transverse polarization around the applied field is extracted, whose corresponding current intensity is known in advance. As long as the oscillation field is maintained perpendicular to the net ambient field, the coil constants in three dimensions could be figured out. This method could effectively avoid the position error since it is employed exactly where the pumping light and the probe light encountered.

2. Principle

The electron spins of K atoms are polarized by a circularly polarized laser tuned to D1 line of K to reduce the fictitious magnetic field induced by AC stark effect [18, 19]. To obtain more uniform spin polarization across the cell, K-Rb hybrid pumping technique is employed to transfer spin polarization from K atoms to Rb atoms [20, 21]. Then, the transmitted linearly-polarized probe laser, slightly detuned from D2 line of Rb due to both effects of the optical rotation and absorption, is modulated by the Rb atoms. The typical Bloch equation describing the evolution of the atomic spin **S** in a magnetic field **B** is as

$$\frac{d}{dt}\mathbf{S}=\gamma\mathbf{B}\times\mathbf{S}+\frac{1}{\mathrm{q}}\left[R_{\mathrm{OP}}\left(\frac{1}{2}\mathrm{s}\hat{\mathbf{z}}-\mathbf{S}\right)-R_{\mathrm{rel}}\mathbf{S}\right] \quad (1)$$

where $\gamma=\gamma^{\mathrm{e}}/(2I+1)$ is the gyromagnetic ratio of the probed atomic state, γ^{e} is the gyromagnetic ratio of the bare electron, and I is the nuclear spin number [22]. The electron spin is coupled to the nuclear spin of alkali metal atoms and has to drag it

while precessing. Therefore, the equivalent gyromagnetic ratio is slower than that of a bare electron. The nuclear slowing down factor q depends on the nuclear spin and the polarization. Considering the stable pumping condition, the nuclear slowing down factor is treated as a constant here. R_{OP} is the pumping rate, R_{rel} is the total relaxation rate, and s is the optical pumping vector along the pump laser propagation direction, with a magnitude of the circular polarization degree. The latter two terms of (1) represent the optical pumping effect and the depolarization effect, respectively.

When an ambient field $\mathbf{B}_0=(\omega_0/\gamma)\hat{\mathbf{z}}$ and an oscillating field $\mathbf{B}'=B'\cos(\omega t)\hat{\mathbf{y}}$ are applied, the transverse response S_x can be obtained from the real part of the solution of (1), whose in-phase component $S_{\text{in-phase}}$ and quadrature component $S_{\text{quadrature}}$, relative to the transverse oscillation field, are as

$$S_{\text{in-phase}}=\frac{S_0(\gamma B'/2)T_2}{1+(\gamma B'/2)^2T_1T_2+(\omega-\omega_0)^2T_2^2} \tag{2}$$

$$S_{\text{quadrature}}=\frac{-S_0(\omega-\omega_0)(\gamma B'/2)T_2^2}{1+(\gamma B'/2)^2T_1T_2+(\omega-\omega_0)^2T_2^2} \tag{3}$$

where T_1 and T_2 are the longitudinal and transverse spin relaxation lifetime, S_0 represents the atomic spin polarization without oscillating excitation, ω is the oscillation frequency, and ω_0 is the Larmor frequency [23]. Larmor frequency can be extracted from either the amplitude-frequency response $S^{(R)}$ or the phase-frequency response $S^{(P)}$. As can be seen in Fig. 1(a), the amplitude-frequency response in practical experiments may suffer from a weak response signal and relatively large noise when the spin polarization is not sufficiently large. Hence, it may be hard to extract an accurate resonance frequency by fitting. Increasing the transverse oscillation field to gain signal strength will lead to a distorted response curve. In contrast, the phase-frequency response presented in Fig. 1(b), which is insensitive to the variation of transverse oscillation field magnitude, has higher signal-to-noise ratio. Common coefficient fluctuations of $S_{\text{in-phase}}$ and $S_{\text{quadrature}}$ components are also suppressed in the phase-frequency response.

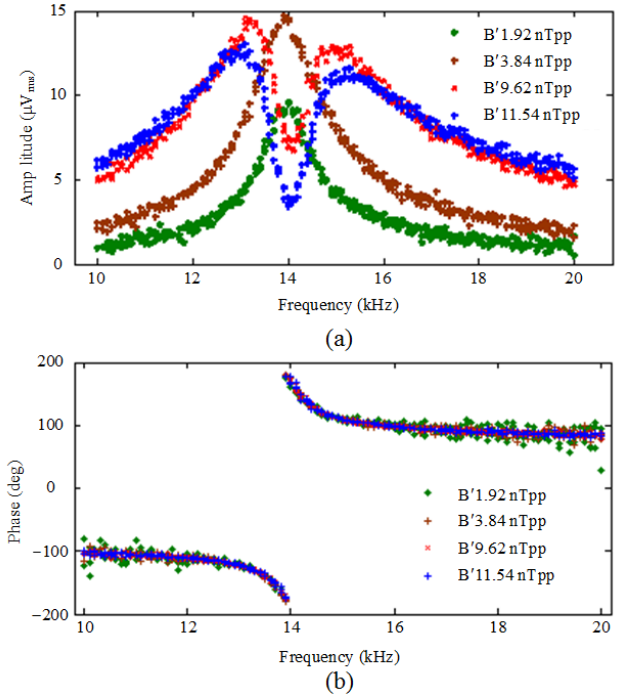

Fig. 1 Experimental magnetic resonance responses: (a) amplitude-frequency responses of a K magnetometer acquired experimentally under 170 ℃, with the pumping power of 109 μW, a static field B_z of 2000 nT and four transverse oscillation fields B': 1.92 nT_{pp} in green, 3.84 nT_{pp} in brown, 9.62 nT_{pp} in red, and 11.54 nT_{pp} in blue and (b) phase-frequency curves under the same conditions.

Therefore, the phase-frequency response $S^{(P)}$ is chosen to figure out the Larmor precession frequency reflecting the magnitude of the applied magnetic field as follows:

$$S^{(P)}=\arctan\left(\frac{S_{\text{in-phase}}}{S_{\text{out-of-phase}}}\right)=\arctan\left(\frac{-1/T_2}{\omega-\omega_0}\right). \tag{4}$$

According to this, ω_0 and subsequently the magnitude of the applied ambient field $B_0=\omega_0/\gamma$ can be achieved. Combined with the known current strength I, the coil constant (the ratio of the applied magnetic field to the applied current) of a certain axis can be determined as $C_{\text{coil}}=B_0/I$.

3. Experimental results and discussion

Figure 2 shows the experimental setup. An external-cavity diode laser (ECDL) (model 6910,

New Focus, USA) is used as the pump laser, whose power is 208 mW and beam diameter is 13 mm. Its wavelength is stabilized at the D1 line (770.108 nm) of K. A distributed-feedback (DFB) laser (model DL100 DFB-L, Toptica, Germany) with 3.8 mW power is chosen as the probe light, with the wavelength tuned to 795.475 nm, close to the D1 line of Rb (795 nm). A 25 mm diameter spherical cell contained K and Rb hybrid vapor with the density ratio of approximately 1:180, 50 torr N_2 and 2.5 atm ^{4}He. The N_2 serves as a quencher absorbing the emitted photons from electrons decaying from excited state to ground state so as to avoid radiation trapping. The ^{4}He serves as buffer gas to minimize diffusion relaxation. A temperature of 473 K is obtained utilizing 99 kHz AC heating current. The residual magnetic fields are compensated after manual zeroing procedures [24]. A set of permalloy four-layer cylindrical magnetic shielding is implemented outside the coils. The optical rotation angle is observed by a balanced photo-detector (model 2307, New Focus, USA).

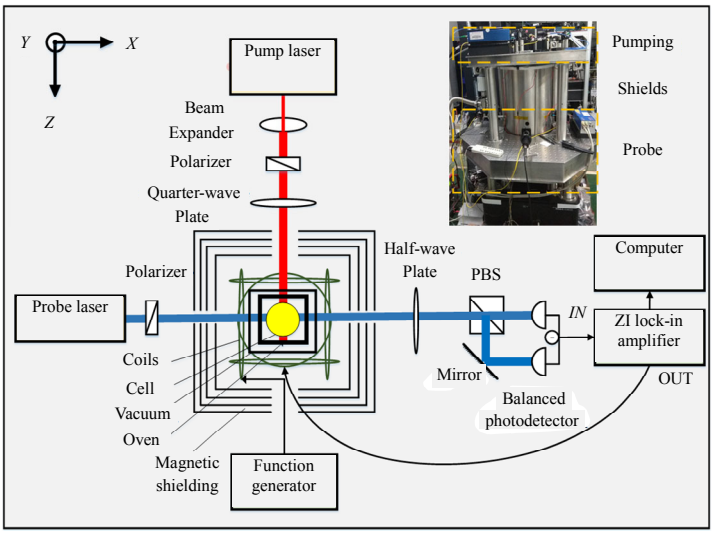

Fig. 2 Schematics of the experimental setup. The inset in the upper right corner is the photograph of the magnetometer. From top to the bottom are the pumping light path, the magnetic shields with sensing unit inside, and the probe light path.

Currents with different intensities are exerted along one of the three directions to generate a bias magnetic field. Meanwhile, coils in a perpendicular direction are linked to the output port of a lock-in amplifier (Zurich Instrument HF2LI) to sweep oscillating field of sine waves. Since the current is known and the corresponding applied magnetic field could be determined from the phase-frequency responses, the magnetic coil constant could be obtained along three directions, respectively.

Equation (4) shows that the magnetic resonance phase-frequency response is symmetrical about the resonance frequency. Therefore, it is theoretically feasible to use one half of the phase-frequency curve to calculate the coil constants for convenience. In this paper, the right halves of the curves are selected and fitted. Figures 3(a) to 3(c) present the representative phase-frequency responses in three directions and their corresponding fittings based on (4), from which the Larmor precession frequency of the electron spins could be achieved. Firstly, the current of 1 mA is applied in the Z direction coil, and the oscillation field is swept along the Y axis. The resonance frequency of 1022 Hz is acquired after fitting the phase-frequency response shown in Fig. 3(a), which means the applied field $B_Z = \omega_Z / \gamma$ has the magnitude of 219 nT. Then, holding on the Z axis bias field, another current of 1.5 mA is added along the Y axis, and the transverse oscillation field is transferred to the X axis. After fitting the

phase-frequency response in Fig. 3(b), the resonance frequency of 1250 Hz is obtained, corresponding to the net bias field B_{YZ} of 267 nT. Considering the applied B_Z of 219 nT, B_Y is figured out to be 154.2 nT according to

$$B_Y = \sqrt{B_{YZ}^2 - B_Z^2} \ . \tag{5}$$

Afterwards, the current in the Y direction is removed, and the current of 3.77 mA is applied in the X direction. The transverse oscillation field is swept along the Y direction. Achieved from the curve in Fig. 3(c), this resonance frequency is 2913 Hz, denoting B_{XZ} of 624 nT and B_X of 584.5 nT, obtained as follows:

$$B_X = \sqrt{B_{XZ}^2 - B_Z^2} \ . \tag{6}$$

To reduce measurement error in each direction, the applied current is varied, whose intensities are within –6.8 mA to –2.3 mA, –3.8 mA to 3.8 mA, and –3 mA to 2.5 mA in the X, Y, and Z direction coils, respectively. The corresponding ambient fields are acquired through magnetic resonance phase-frequency analysis. Each measurement represents one point in Figs. 4(a) to 4(c). The coil constant C_{coil} is obtained by fitting these points as

$$\left|B_{\text{total}}\right| = \left|C_{\text{coil}}\, I + B_{\text{residual}}\right| \tag{7}$$

where B_{total} is the field sensed by spin polarization, and B_{residual} is the residual field inside the shielding barrel.

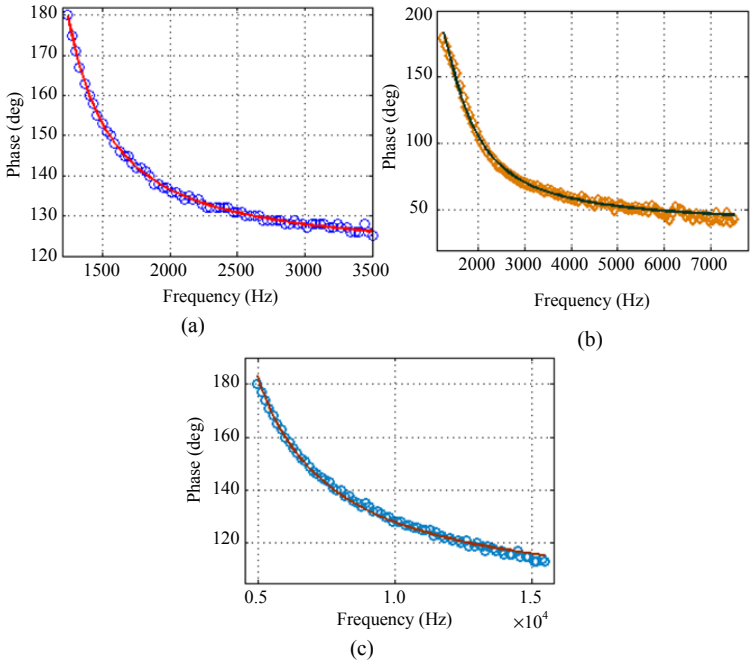

Fig. 3 Phase-frequency responses and fitting results in three directions: (a) phase-frequency response and fitting results under currents of 1 mA in the Z direction, with adjusted R^2 of 0.9984 and the resonance frequency of 1022 Hz, corresponding to B_Z of 219 nT, (b) phase-frequency response and fitting results under currents of 1 mA in Z direction and 1.5 mA in the Y direction, with adjusted R^2 of 0.9946 and the resonance frequency of 1250 Hz and B_Y of 154.2 nT, and (c) phase-frequency response and fitting results under currents of 1 mA in Z direction and –3.77 mA in the X direction, with adjusted R^2 of 0.9952 and the resonance frequency of 2913 Hz and B_X of 584.5 nT.

Figure 4 presents the linear relationship of the currents and corresponding field magnitudes in three directions, from which the coil constants of the triaxial coil system are achieved. To realize magnetic resonance, an ambient field current of 1 mA is maintained in the Z axis. Under this condition, however, small B_X and B_Y components could barely contribute to the total field B_{total}. Since that, currents of large intensities are adopted in the X and Y directions. The curves coincided well with the

data using (7). The adjusted R^2 of linear fittings for the X, Y, and Z axes are 0.9893, 0.9776, and 0.9256, respectively. Also, the error of coil constant is calculated on each current point according to $\Delta C_i = \left(C_{\text{coil}} I_i + B_{\text{residual}} - B_{\text{total}}\right) / I_i$, and then the mean error is figured out to illustrate the calibration accuracy [16, 25]. The coil constant in the X direction is approximately 323.1 nT/mA, with a mean error of 0.28 nT/mA. The coil constant in the Y direction is 108 nT/mA, with a mean error of 0.04 nT/mA. The coil constant in the Z direction is 185.8 nT/mA, with a mean error of 1.03 nT/mA. The residual fields are also obtained from fittings with the number of 6.367 nT, 2.915 nT, and 47.67 nT in the X, Y, and Z directions, respectively, which mainly come from insufficient or over compensation from the zeroing procedures. The root mean square error (RMSE) of fitting these three curves are 54.67 nT, 15.94 nT, and 46.65 nT in the X, Y, and Z directions, respectively.

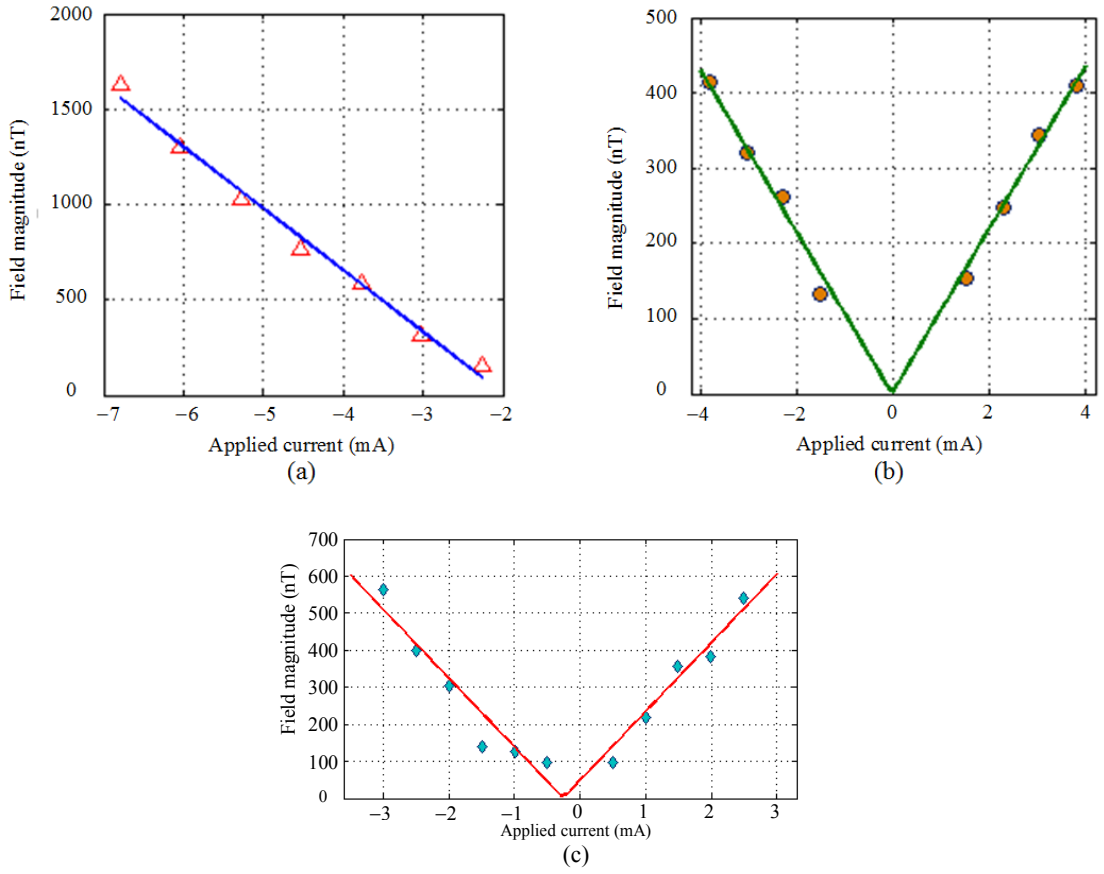

Fig. 4 Linear relationship between the applied current intensities and the sensed field magnitudes in three directions. The dots represent the obtained field from phase-frequency analysis, and the solid line represents the fitting curve: (a) the linear coil constant fitting in the X axis, (b) the linear coil constant fitting in the Y axis, and (c) the linear coil constant fitting in the Z axis.

4. Conclusions

In this paper, we put forward a method to calibrate the coil constants of three axes performed on alkali atomic magnetometers. This method is built on measuring the Larmor precession frequency of atoms through phase-frequency analysis. The coil constants could be calibrated by measuring the magnetic field magnitudes under known applied currents. This method operates with electron spins of alkali metal, instead of nuclear spins of noble gas. It is carried out directly on the magnetometer, thus avoiding the effects of the position error. We experimentally demonstrate this method on a K-Rb hybrid atomic magnetometer. The coil constant measurement results are 323.1 ± 0.28 nT/mA,

108 ± 0.04 nT/mA and 185.8 ± 1.03 nT/mA along the *X*, *Y*, and *Z* directions, respectively.

Acknowledgement

This work received the support of the National Key R&D Program of China (Grant No. 2017YFB0503100) and the National Natural Science Foundation of China (NSFC) (Grant No. 61227902). Both these two funding agencies give suggestions on selecting the critical technical problems and official financial help on the implementation of experiments.

References

[1] I. K. Kominis, T. W. Kornack, J. C. Allred, and M. V. Romalis, "A subfemtotesla multichannel atomic magnetometer," *Nature*, 2003, 422(6932): 596–599.

[2] J. C. Allred, R. N. Lyman, T. Kornack, and M. Romalis, "High-sensitivity atomic magnetometer unaffected by spin-exchange relaxation," *Physical Review Letters*, 2002, 89(13): 130801-1–130801-4.

[3] Y. Chen, W. Quan, L. H. Duan, Y. Lu, L. W. Jiang, and J. C. Fang, "Spin-exchange collision mixing of the K and Rb ac Stark shifts," *Physical Review A*, 2016, 94(52): 052705-1–052705-6.

[4] D. Sheng, S. Li, N. Dural, and M. Romalis, "Subfemtotesla scalar atomic magnetometry using multipass cells," *Physical Review Letters*, 2013, 110(16): 160802-1–160802-5.

[5] T. H. Sander, J. Preusser, R. Mhaskar, J. Kitching, L. Trahms, and S. Knappe, "Magnetoencephalography with a chip-scale atomic magnetometer," *Biomedical Optics Express*, 2012, 3(5): 981–990.

[6] R. Wyllie, M. Kauer, G. S. Smetana, R. T. Wakai, and T. G. Walker, "Magnetocardiography with a modular spin-exchange relaxation-free atomic magnetometer array," *Physics in Medicine & Biology*, 2012, 57(9): 2619–2632.

[7] T. Wang, D. F. J. Kimball, A. O. Sushkov, D. Aybas, J. W. Blanchard, G. Centers, *et al.*, "Application of spin-exchange relaxation-free magnetometry to the cosmic axion spin precession experiment," *Physics of the Dark Universe*, 2018, 19: 27–35.

[8] J. M. Brown, "A new limit on Lorentz- and CPT-violating neutron spin interactions using a potassium-Helium comagnetometer," Ph.D. dissertation, Princeton University, Princeton, NJ, USA, 2011.

[9] Z. C. Ding, J. Yuan, G. F. Lu, Y. Y. Li, and X. W. Long, "Three-axis atomic magnetometer employing longitudinal field modulation," *IEEE Photonics Journal*, 2017, 9(5): 5300209-1–5300209-9.

[10] H. C. Huang, H. F. Dong, X. Y. Hu, L. Chen, and Y. Gao, "Three-axis atomic magnetometer based on spin precession modulation," *Applied Physics Letters*, 2015, 107(18): 227–234.

[11] S. Afach, G. Ban, G. Bison, K. Bodek, Z. Chowdhuri, Z. Gruji´c, *et al.*, "Highly stable atomic vector magnetometer based on free spin precession," *Optics Express*, 2015, 23(17): 22108-1–22108-12.

[12] H. F. Dong, H. B. Lin, and X. B. Tang, "Atomic-signal-based zero-field finding technique for unshielded atomic vector magnetometer," *IEEE Sensors Journal*, 2013, 13(1): 186–189.

[13] Z. M. Li, R. T. Wakai, and T. G. Walker, "Parametric modulation of an atomic magnetometer," *Applied Physics Letters*, 2006, 89(13): 23575531-1–23575531-8.

[14] S. J. Seltzer and M. Romalis, "Unshielded three-axis vector operation of a spin-exchange-relaxation-free atomic magnetometer," *Applied Physics Letters*, 2004, 85(20): 4804–4806.

[15] H. U. Auster, K. H. Glassmeier, W. Magnes, O. Aydogar, W. Baumjohann, D. D. Constantinescu, *et al.*, "The THEMIS fluxgate magnetometer," *Space Science Reviews*, 2008, 141(1–4): 235–264.

[16] H. Zhang, S. Zou, and X. Y. Chen, "A method for calibrating coil constants by using an atomic spin co-magnetometer," *The European Physical Journal D*, 2016, 70(10): 203-1–203-5.

[17] L. L. Chen, B. Q. Zhou, G. Q. Lei, W. F. Wu, J. Wang, Y. Y. Zhai, *et al.*, "A method for calibrating coil constants by using the free induction decay of noble gases," *AIP Advance*s, 2017, 7(7): 2227–2234.

[18] Y. Li, M. Ding, X. J. Liu, H. W. Cai，J. P. Zhao, and J. C. Fang, "Suppression method of AC-stark shifts in atomic magnetometers," *IEEE Photonics Journal*, 2018, 10(5): 5300207-1–5300207-5.

[19] J. X. Lu, W. Quan, D. Ming, L. Qi, and J. C. Fang, "Suppression of light shift for high-density alkali-metal atomic magnetometer," *IEEE Sensors,* 2018, 99: 2877771-1–2877771-5.

[20] M. Romalis, "Hybrid optical pumping of optically dense alkali metal vapor without quenching gas,"

Physical Review Letters, 2010, 105(24): 243001-1–243001-4.

[21] Y. Ito, H. Ohnishi, K. Kamada, and T. Kobayashi, "Development of an optically pumped atomic magnetometer using a K-Rb hybrid cell and its application to magnetocardiography," *AIP Advances*, 2012, 2(3): 032127-1–032127-4.

[22] F. Bloch, W. W. Hansen, and M. E. Packard, "The nuclear induction experiment," *Physics Review*, 1946, 70(7–8): 474–485.

[23] S. Seltzer, "Developments in alkali metal atomic magnetometry," Ph.D. dissertation, Princeton University, Princeton, NJ, USA, 2008.

[24] J. Fang, T. Wang, W. Quan, H. Yuan, Y. Li, H. Zhang, *et al.*, "In situ magnetic compensation for potassium spin-exchange relaxation-free magnetometer considering probe beam pumping effect," *Review of Scientific Instruments*, 2014, 85(6): 063108-1–063108-7.

[25] L. L. Chen, B. Q. Zhou, G. Q. Lei, W. F. Wu, Y. Y. Zhai, Z. Wang, *et al.*, "A method for measuring the spin polarization of ^{129}Xe by using an atomic magnetometer," *AIP Advances*, 2017, 7: 085221-1–085221-8.